CONF-78-139-E
1 0045

E45A

The University of Michigan

THE HARRISON M. RANDALL LABORATORY OF PHYSICS • ANN ARBOR, MICHIGAN 48109
(313) 764-4437

RECEIVED
OCT 12 1978
DIRECTORS OFFICE
FERMILAB

UMBC 78-9

(August 1978)

EXPERIMENTAL PROPERTIES OF NEUTRINO-INDUCED JETS

J. C. Vander Velde

University of Michigan

Berkeley-Hawaii-Fermilab-Michigan Collaboration

This paper is a reproduction of a talk given at the Symposium on Jets in High Energy Collisions, Neils Bohr Institute, Copenhagen, Denmark (July 1978)

EXPERIMENTAL PROPERTIES OF NEUTRINO-INDUCED JETS

J. C. Vander Velde

Berkeley-Hawaii-Fermilab-Michigan Collaboration

J. Bell, C. T. Coffin, R. N. Diamond[†], H. T. French[‡], W. C. Louis, B. P. Roe, R. T. Ross, A. A. Seidl, J. C. Vander Velde, E. Wang

University of Michigan
Ann Arbor, Michigan 48109

J. P. Berge, D. V. Bogert, F. A. DiBianca[‡], R. Hanft, C. Kochowski[*], J. A. Malko, G. I. Moffatt[#], R. Endorf[#], F. A. Nezrick, W. G. Scott[††], W. Smart

Fermi National Accelerator Laboratory
Batavia, Illinois 60510

R. J. Cence, F. A. Harris, M. Jones, M. W. Peters, V. Z. Peterson, V. J. Stenger

University of Hawaii at Manoa
Honolulu, Hawaii 96822

G. R. Lynch, J. P. Marriner, M. L. Stevenson

Lawrence Berkeley Laboratory
Berkeley, CA. 94720

[†]Present address: Florida State University, Tallahassee, FL.

[‡]Present address: Columbia University, New York, N.Y. 10027

[‡]Present address: General Electric Company, Milwaukee, WIS.

[††]Present address: CERN, Geneva 23, Switzerland

[*]Present address: CEN Saclay, France

[#]Visitors from the University of Cincinnati, OHIO

ABSTRACT

Experimental properties of neutrino-induced jets. J.C. Vander Velde

We analyze a sample of about 2000 charged-current neutrino-proton interactions with neutrino energy greater than 10 GeV produced in the 15-ft. hydrogen bubble chamber at Fermilab using a broad band neutrino beam. We study the details of the hadrons produced and find generally good agreement with the quark-parton model and present parametrizations of quark fragmentation (D) functions. The D functions are found to be independent of Q^2 and W (total hadronic mass) for W > 4 GeV, in agreement with the model. The height of the rapidity plateau in the quark (current) fragmentation region is compared to that of the di-quark (target) fragmentation region and the two are found to agree. The mean transverse momentum P_T of the hadrons is studied for its Q^2 and Feynman-X dependence. We find a sizeable increase of $\langle P_T^2 \rangle$ with Feynman-X which agrees, however, with our longitudinal phase space model. We find no statiscally significant dependence of $\langle P_T^2 \rangle$ on Q^2, up to $Q^2 = 64$ GeV^2, although the highest momentum hadrons are consistent with a mild Q^2 dependence. There are no effects of high "primordial" parton momentum apparent in the data. No effects of gluon radiation are found in the Q^2 dependence of the phase space density of particle production near zero c.m. rapidity.

1. Introduction

I will discuss some results on the properties of single and correlated hadrons made in the hadron "jet" via the reaction

$$\nu p \rightarrow \mu^- + \text{jet}$$

We know the direction of the jet to within ± 1° in these events and the individual charged hadrons' vector momenta are measured to better than a few percent. Hence we have an excellent method to study the detailed properties of hadron jets.

The elementary process that forms the jets is believed to be the interaction of a virtual W^+ weak boson with a d quark in the proton--changing it to a u quark. In the c.m. of the overall hadronic system we can picture this as follows:

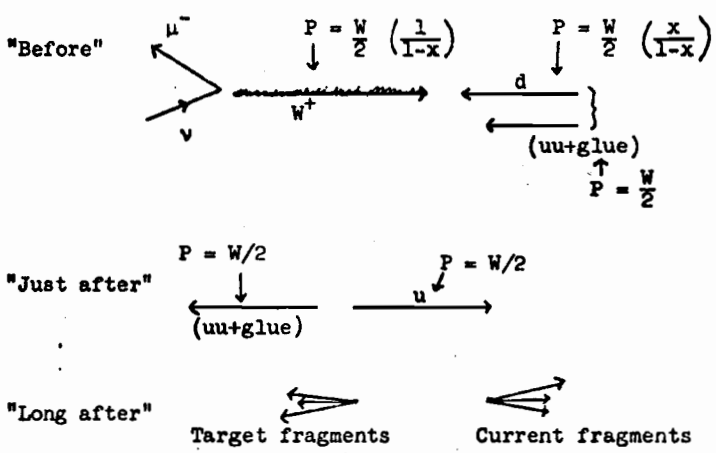

Looked at in this way, each event consists of a pair of back-to-back jets; one formed from the fragmentation of a

u quark and the other formed from the spectator remains of the target proton which consists of two u quarks and some gluons, $q\bar{q}$ pairs, etc. We have indicated on the diagram the momenta of these elemental objects, before and after the collision, expressed in terms of the overall invariant hadronic mass W and the Bjorken scaling variable x.

2. Basic Properties

We will start by showing a few of the general properties of the jets we observe. Our data indicate that the properties of the "current jet" and the "target jet" are quite similar. In Fig. 1 we compare the rates of hadron production vs. rapidity in the two regions and find that they are equal within statistics. (The cuts are made in order to separate the two regions). This may indicate that in purely hadronic processes the jet formed by a single quark emanating from a hard scattering will be similar to the diquark jet formed by the remains of the parent nucleon.

The angular confinement of the total hadronic system, if we think of it as a single "jet", is illustrated in Fig. 2. The larger the jet momentum, the smaller is the fraction of its energy that appears outside a given lab angle. Fig. 2 should give the hadron jet experimenter a rough idea of what fraction of the jet's energy can be captured in a fixed-angle apparatus.

The fraction of longitudinal momentum carried by the first and second highest momentum particles is shown in Fig. 3.

(Figs. 2 and 3 are smooth curves drawn through the data). The data of Fig. 3 also scale in the sense that the fraction of the remaining momentum carried by the "second" (ignoring the "first") is distributed (not shown) just like the fraction of the total that the "first" carries.

We now turn to some more details of these events looked at in the context of the quark-parton model. The W distribution for 1670 events (which we believe to be ~ 95% pure νp charged current) is shown in Fig. 4. The cuts shown on the figure are made to purify the charged current (CC) sample. They are described in detail in Ref. 1. The sharp peak near 1 GeV represents the exclusive channel $\nu p \to \mu^- + (\Delta^{++} \to p\pi^+)$.

According to Feynman's idea [2] a given struck quark should develop into a jet of hadrons ("fragment") in a way which is independent of the kinematic variables (W and Q^2) associated with its formation. In Fig. 5 we see that the average number of charged particles is indeed independent of Q^2 for various W values. Fig. 6 indicates that the number of positive and negative high Z hadrons per event changes with W for low W values but appears to approach a constant plateau for $W \gtrsim 4$ GeV. Hence one of the basic assumptions of the quark-parton model - that quark fragmentation is independent of W and Q^2 - is confirmed by Figs. 5 and 6, at least for $W \gtrsim 4$ GeV and $2 < Q^2 < 64$ GeV^2. (Z is the longitudinal fraction of total hadronic momentum carried by a given hadron.)

The solid curves on Fig. 6 are from a Monte Carlo calculation described in detail in Ref. 1. The calculation is meant to account for the "kinematic" effects of longitudinal

phase space and charge conservation, and so it generates hadrons with a flat distribution in (the W rest frame) rapidity and an exponential in the transverse mass but no charge-neutral or charge-charge correlations (e.g. clusters or resonances) are put in. We refer to the model calculations as "uncorrelated Monte Carlo" (UMC). The generated events are passed through the same event reconstruction procedures and cuts as the real events and thus allow us also to evaluate our biases.

Encouraged by the Q^2 independence and Feynman scaling properties of the events (Figs. 5, 6 we proceed to examine further details of these back-to-back quark-diquark systems. The first thing we note is that they have a definite jet-like character , as illustrated in Fig. 7. We plot the average value of P_T^2 vs. W for particles in two different Feynman X (X_F) regions. In both regions $\langle P_T^2 \rangle$ rapidly attains a maximum value which is much less than its kinematically allowed value of $W^2/4$. This means that we are indeed observing "jets" with a severely limited transverse momentum distribution not unlike that of the exponentially cut-off UMC model in which $d^2\sigma/dYdP_T^2 = e^{-bm_T}$ (with m_T = transverse mass and $b = 6$ GeV^{-1}). We will say more about the Q^2 and X_F dependence of $\langle P_T^2 \rangle$ later.

3. Longitudinal Properties

The single particle inclusive properties of the quark-diquark jet can be examined in terms of longitudinal, transverse, and azimuthal variables. In order to deal only with events in the scaling region of Fig. 6, we make a "high W" selection of $W > 4$ GeV in addition to the selections shown

on Fig. 4. The resulting distributions for h^- and h^+ hadrons are shown plotted vs. the longitudinal X_F variable in Figs. 8 and 9. We see that both distributions, and hence their ratio, are fairly well represented by the UMC model. This indicates that a quark fragments into hadrons in a manner which approximates longitudinal phase space in its single particle inclusive aspects. Figs. 8 and 9 represent the so-called D functions of Feynman [2] integrated over transverse momentum and using X_F instead of Z as the longitudinal variable.

4. Charge Distribution

Field and Feynman suggest (FF2)[3] that when a high energy quark fragments its properties will be most strongly correlated to those of the highest momentum ("fastest") hadron observed. They have made predictions for the distribution in Z_R of the fastest positive and fastest negative hadron in each event, where Z_R is the fraction of the total charged hadron momentum carried by the fastest charged hadron. These predictions for a fragmenting u quark are shown in Fig. 10, and are in good agreement with the data. We also show the UMC calculation. It is somewhat surprising that the UMC model gives such a good description, since it has no input charge correlations other than those arising from charge conservation. The difference between the fastest positive and the fastest negative distributions in the UMC arises solely from the fact that there are more positives than negatives generated in each event, and hence the fastest one is more likely to be positive.

This difference between positives and negatives will diminish at higher W values but the predicted change with W is slow due to the logarithmic increase in charged particle multiplicity put into the UMC model. In any case, at our present energies, Fig. 10 does <u>not</u> give evidence for the charge of a fragmenting u quark, but simply reflects overall charge conservation in the events.

5. Transverse Momentum Properties

We now examine the transverse momentum (P_T) properties of the produced hadrons relative to the overall hadronic (virtual W^+) direction in the lab. This is of interest in looking for effects of gluon bremsstrahlung from the struck quark and/or "primordial" parton momentum in the struck proton. Such effects are conjectured to cause $\langle P_T \rangle$ to be an increasing function of Q^2 and Feynman X_F. We see in Fig. 11a that $\langle P_T^2 \rangle$ is indeed a steep function of X_F. However this is primarily due to the kinematic "seagull effect" and disappears if we choose another longitudinal variable such as Y_q (Fig. 11b). The curves on Fig. 11 are from the UMC model calculation and illustrate that the P_T properties of the bulk of the produced particles can be nicely described by longitudinal phase space (LPS). If we are to look for any anamolous effects of gluons we must first understand and account for the seagull effect. Not doing so has often been a source of some confusion in this subject.

The seagull effect can be easily understood from Fig. 12 which shows lines of constant c.m. rapidity (Y) on a $Z_\perp$ vs. X

plot (on the right) and lines of constant X on a $Z_\perp$ vs. Y plot (on the left). Imagine that particles populate the plot on the left with a density which is independent of Y (up to the kinematic boundary) but decreasing with the transverse variable $Z_\perp = 2\sqrt{m^2+P_T^2}/W$ in accordance with LPS. If we calculate $\langle P_T \rangle$ vs. Y we simply get a flat function which tails off at large Y due to the kinematic boundary. However, if we plot $\langle P_T \rangle$ vs. X for the same data we get a "seagull". This is because, looking at the two adjacent horizontal bars on Fig. 12, at a given P_T (or $Z_\perp$) the production rate is proprotional to ΔY, and ΔY is a decreasing function of X for a fixed ΔX ($\Delta Y = \Delta X/\sqrt{X^2+Z_\perp^2}$). I.e., the inner bar (X = 0 to .1) contains more particles than the one adjacent to it (X = .1 to .2) and therefore low P_T is more heavily weighted in the low X interval. Hence the seagull effect arises simply from LPS and the transformation of variables giving $dY = dX/\sqrt{X^2+Z_\perp^2}$. It even produces the surprising result that $\langle P_T \rangle$ (X = 0) is less than $\langle P_T \rangle$ (Y = 0) along the <u>same line</u> X = Y = 0!

Turning back to Fig. 11a we see that the data show no significant X-dependent increase of $\langle P_T^2 \rangle$ above what is expected from LPS (solid line). To look further for effects of gluon emission we take events in which the highest momentum (h_1) track is positive and therefore most closely related kinematically to the parent u quark. If we plot $\langle P_T^2 \rangle$ for these particles vs. Q^2 we do see a rise, but it is practically all accounted for by a similar rise in the UMC calculations (Fig. 13). The QCD - expected linear rise is only vaguely hinted

at with a coefficient $d\langle P_T^2 \rangle/dQ^2 \approx .003 \pm .003$. Still another place where gluon radiation or primordial parton momentum should show up is in the fragmentation region of the target proton which has been stripped of one of its quarks. This kinematic region is best defined in the lab frame where the target is initially at rest. We again focus our attention on positive particles, since are are looking for fragments of a uu diquark, and restrict the particle momentum to $P_{lab} <$ 2 GeV/c. The $\langle P_T^2 \rangle$ for these particles (and also those with $P_{lab} >$ 2 GeV/c) is plotted vs. Q^2 in Fig. 14. Again we find no Q^2-dependent effects up to Q^2 = 64 GeV^2; the data follow the UMC model extremely well. (There are 337 particles from 180 events in the $16 < Q^2 < 64$ region of the $P_{lab} <$ 2 GeV/c data.) If indeed the proton contains primordial parton transverse momentum of order .8-.9 GeV/c, as some hadronic experiments have indicated, it does not appear to manifest itself in these neutrino data. We may be just on the verge of having high enough Q^2 to see these effects, if indeed they are there. Hopefully other deep inelastic and e^+e^- annihilation experiments will settle these questions in the near future.

6. Fragmentation of Gluons?

Virtual gluons, if they "exist", are supposed to produce hadrons jets just as virtual quarks do. If the struck quark in our case emits a gluon one might expect two separate jets to develop in the current fragmentation region. These two separate jets would be difficult to observe at our energies, but one might expect the density of particles in phase space

to increase significantly in such events, and that their frequency would increase with Q^2. Hence we show in Fig. 15 the density of hadrons near $Y = 0$ as a function of Q^2. After an initial rise there seems to be very little Q^2 dependence. Again we must conclude that either the effects of gluon radiation are quite small, and/or we need higher Q^2 values to see them.

I am much indebted to my colleagues of the Berkeley-Hawaii-Fermilab-Michigan E45 collaboration for a lot of hard work in extracting and analyzing these data. In addition I have benefited particularly from conversations with J. D. Bjorken, R. N. Cahn, S. D. Ellis, R. D. Field, G. L. Kane, and H. D. Politzer.

I am most grateful to Knud Hansen and Paul Hoyer for their hard work and hospitality; and the same should be said, I'm sure, for many other unsung heroes who have helped to make this such a fine symposium. I shall also remember fondly how some of us non-heroes were " sung" (literally) at the banquet.

References

[1] Bell, J., Berge, J.P., Bogert, D.V., Cence, R.J., Coffin, C.T., Diamond, R.N., DiBiance, F.A., Endorf, R., French, H.T., Hanft, R., Harris, F.A., Jones, M., Kochowski, C., Louis, W.C., Lynch, G.R., Malko, J.A., Marriner, J.P., Moffatt, G.I., Nezrick, F.A., Peters, M.W., Peterson, V.Z., Roe, B.P., Ross, R.T., Scott, W.G., Seidl, A.A., Smart, W., Stenger, V.J., Stevenson, M. L., Vander Velde, J.C., and Wang, E., Experimental Study of Hadrons Produced in High Energy Charged Current Neutrino-Proton Interactions, University of Michigan preprint UMBC 78-6, (submitted to Physical Review June 1978).

[2] Feynman, R.P., "Photon-Hadron Interactions", Frontiers in Physics series, David Pines, Editor, Published by W. A. Benjamin, Inc., Reading, Mass. (1972).

[3] Field, R.D. and Feynman, R.P., A Parametrization of the Properties of Quark Jets, Nucl. Phys. B (to be published).

Figure Captions

Fig. 1. Charged hadron rate for high-Q^2 events plotted vs. rapidity Y_{lab} and quark-frame rapidity $Y_q = Y_{lab} - \ln(W^2/1\ GeV^2)$. The approach to and height of the two "plateaux" are very similar.

Fig. 2. Fraction of visible energy E_{VIS} contained inside lab angle θ with respect to the entire hadronic system direction.

Fig. 3. Distribution of the fraction Z_R of visible longitudinal momentum carried by the 1st, 2nd, and (1st plus 2nd) highest momentum charged hadrons.

Fig. 4. Distribution of invariant mass of the hadronic system for a sample of neutrino charged-current events. Typical mass resolution is ±15% for the bulk of the events, which have missing neutrals. The peak at the left is due to the final state $\mu^- \Delta^{++}$.

Fig. 5. Average number of charged particles in the hadronic system vs. Q^2 for various W slices taken from Fig. 4. The dashed lines represent the overall average for each W slice.

Fig. 6. The rate of production of positive and negative hadrons with $Z > .2$ as a function of W. We take the Feynman scaling (W-independent) region as $W > 4$ GeV. The curves are the result of the Monte Carlo model described in the text.

Fig. 7. Average value of P_T^2 vs. W for two X_F regions.

Fig. 8 . (a) The (positive/negative) hadron ratio vs. X_F .
(b) The D_u^- function vs. X_F. The average number of negative tracks (integral of the graph) is indicated.

Fig. 9 . The D_u^+ function vs. Feynman X in the hadronic rest frame. Identified (ID) and the estimated misidentified protons are indicated. The normalization of the UMC model is absolute and not adjusted to fit the data.

Fig. 10. (a) and (b). The distribution in $Z_R = P_{\parallel}/P_{visible}$ of the "fastest" positive and negative tracks in each event. The dashed curves are the predictions of Field and Feynman. Fig. 10a includes (+) tracks from events where the fastest track is negative and vice-versa for 10b.

Fig. 11. (a) Average transverse momentum squared vs. Feynman X for charged particles in the $X_F > 0$ (current fragmentation) hemisphere. The seagull effect, seen here is discussed in detail in the text.
(b) $\langle P_T^2 \rangle$ vs. rapidity in the quark frame, $Y_q = Y_{lab} - \ln(W^2/1\ GeV^2)$. $X_F > 0$ corresponds roughly to $Y_q > -2$.

Fig. 12. Kinematic plot to illustrate the seagull effect (see text).

Fig. 13. $\langle P_T^2 \rangle$ vs. Q^2 for h_1 tracks with $Z > .3$ in events where h_1 is (+). There are 497 events (and 497 tracks) in the plot with average Z value $\langle Z \rangle = .45$.

Events with 3 GeV < W < 12 GeV are used. The dashed curve is a fit to a linear function of Q^2 which has been added to the baseline curve (solid) calculated with the UMC model.

Fig. 14. Average transverse momentum-squared of positive hadrons in two P_{lab} regions. Events with W between 4 and 12 GeV are used.

Fig. 15. Particle density near Y = 0 as a function of Q^2.

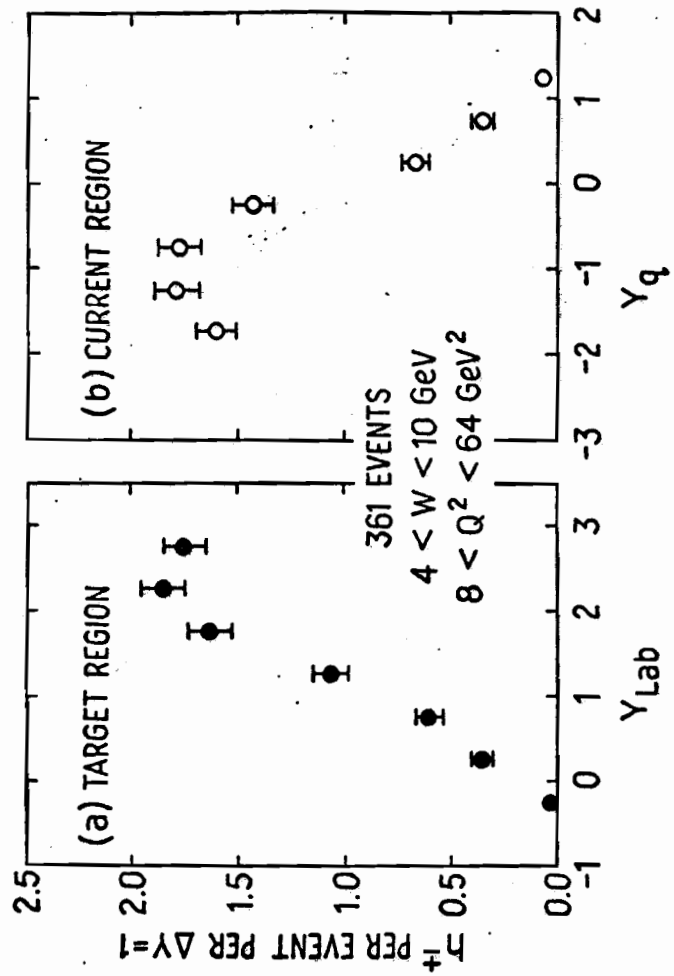

Fig. 1

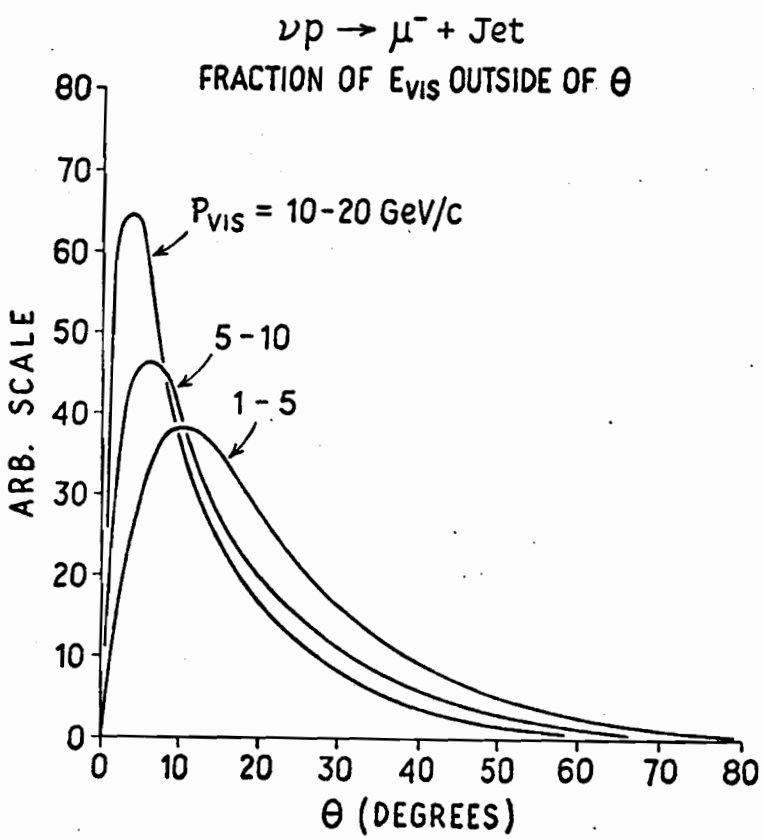
$\nu p \rightarrow \mu^- + \text{Jet}$
FRACTION OF E_{VIS} OUTSIDE OF θ
P_{VIS} = 10-20 GeV/c
5-10
1-5
ARB. SCALE
θ (DEGREES)
0
10
20
30
40
50
60
70
80

Fig. 2

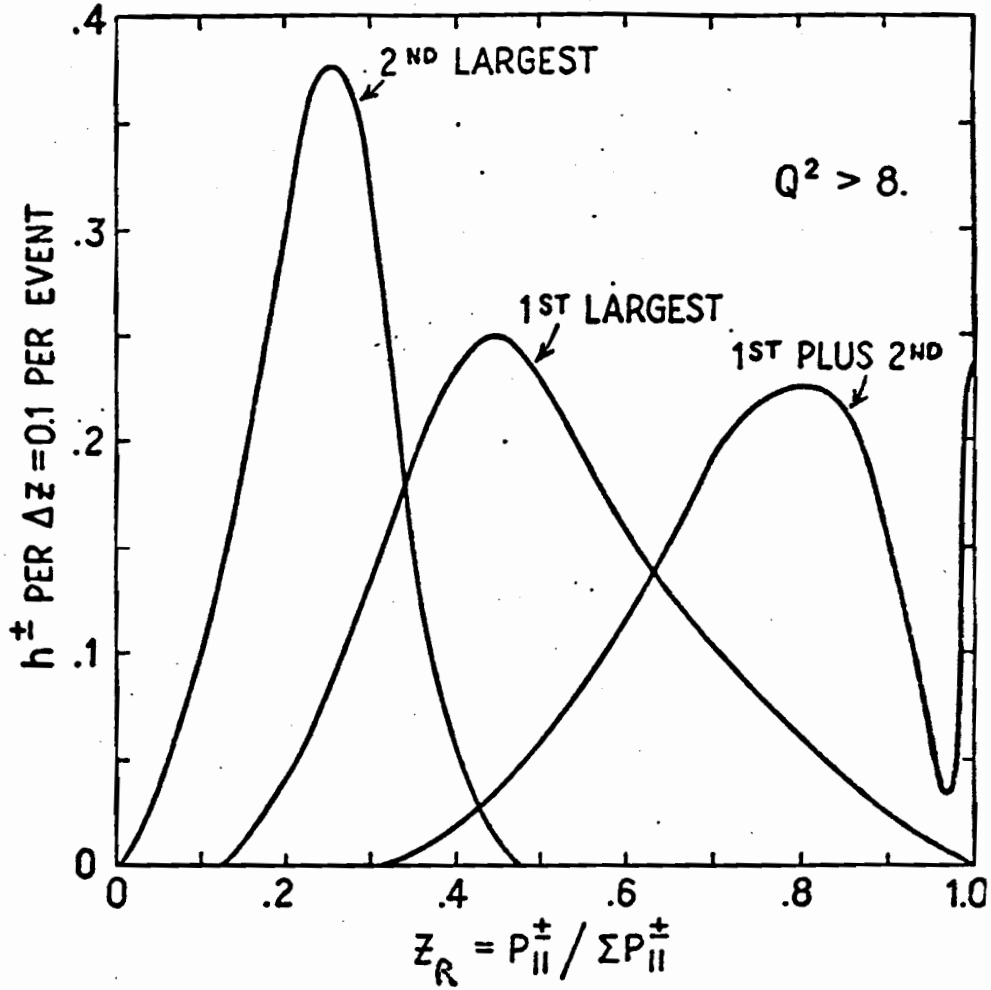
2 ND LARGEST
1ST LARGEST
1ST PLUS 2ND
$Q^2 > 8.$
$h^\pm$ PER Δz=0.1 PER EVENT
$z_R = P_{\parallel}^{\pm} / \Sigma P_{\parallel}^{\pm}$
0
.1
.2
.3
.4
.6
.8
1.0

Fig. 3

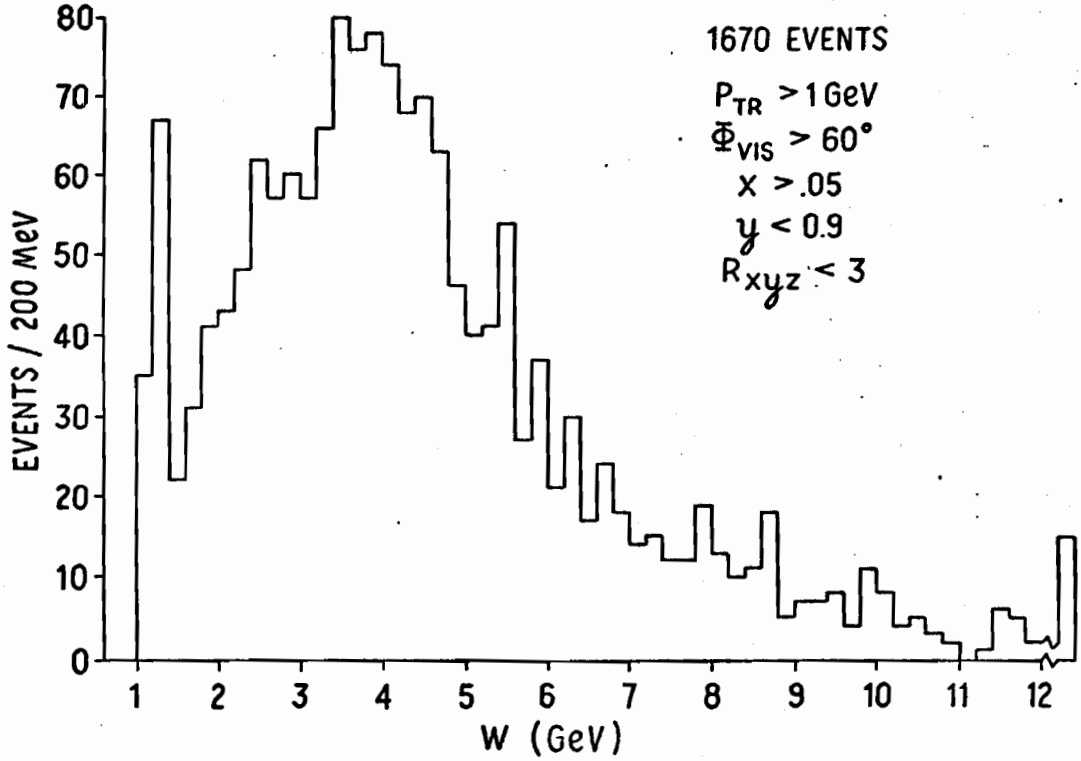
1670 EVENTS
$P_{TR} > 1$ GeV
$\Phi_{VIS} > 60°$
$x > .05$
$y < 0.9$
$R_{xyz} < 3$
EVENTS / 200 MeV
W (GeV)

Fig. 4

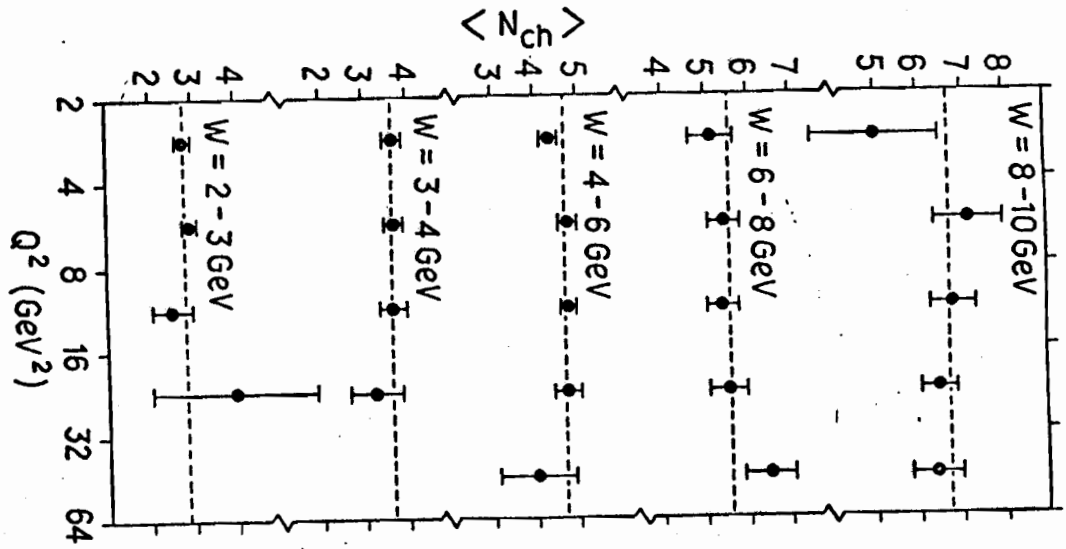
$\langle N_{ch} \rangle$
W = 8 - 10 GeV
W = 6 - 8 GeV
W = 4 - 6 GeV
W = 3 - 4 GeV
W = 2 - 3 GeV
Q^2 (GeV^2)

Fig. 5

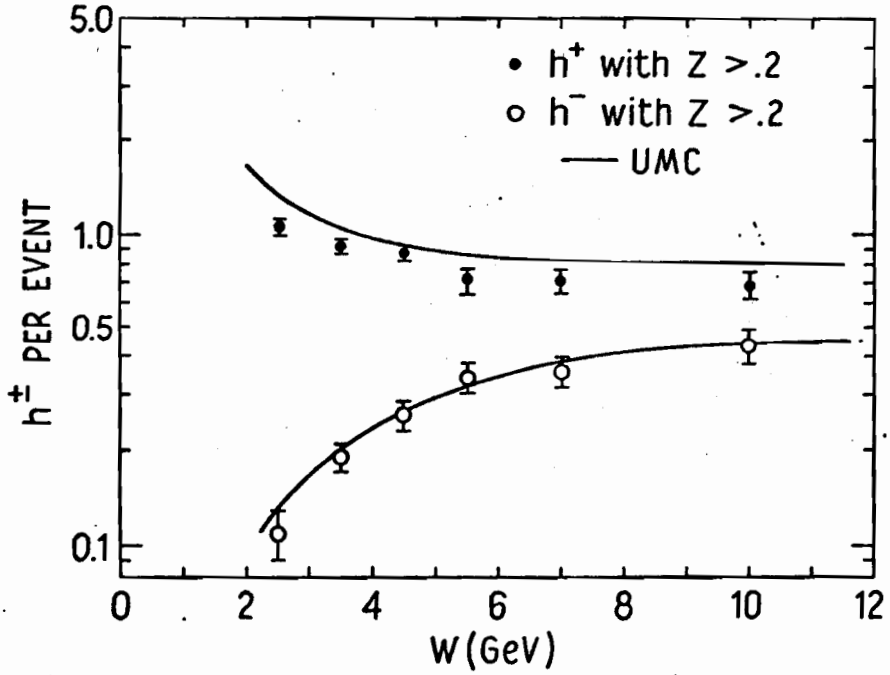
5.0
1.0
0.5
0.1
$h^{\pm}$ PER EVENT
• h^+ with Z >.2
o h^- with Z >.2
— UMC
0
2
4
6
8
10
12
W (GeV)

Fig. 6

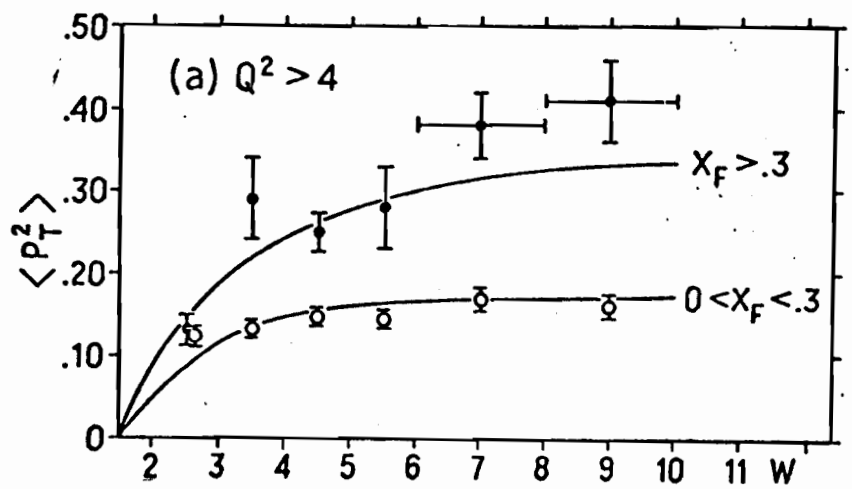
.50
.40
.30
.20
.10
0
$\langle P_T^2 \rangle$
(a) $Q^2 > 4$
$X_F > .3$
$0 < X_F < .3$
2
3
4
5
6
7
8
9
10
11
W

Fig. 7

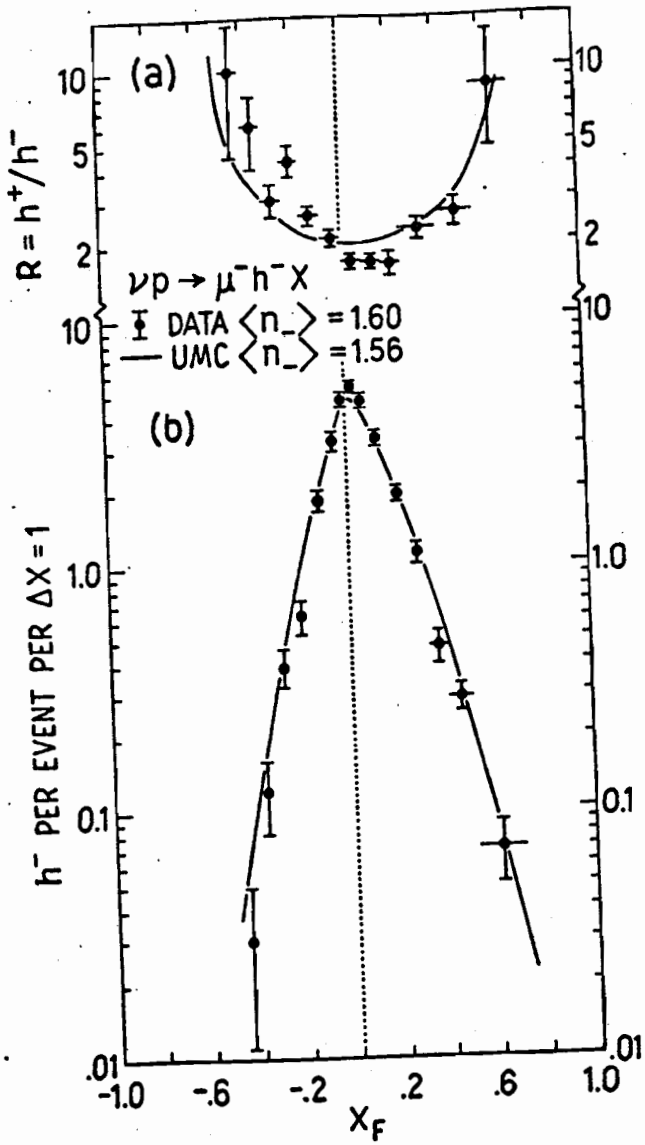
(a)
(b)
$R = h^+/h^-$
$\nu p \to \mu^- h^- X$
DATA $\langle n_- \rangle = 1.60$
UMC $\langle n_- \rangle = 1.56$
h^- PER EVENT PER $\Delta X = 1$
X_F

Fig. 8

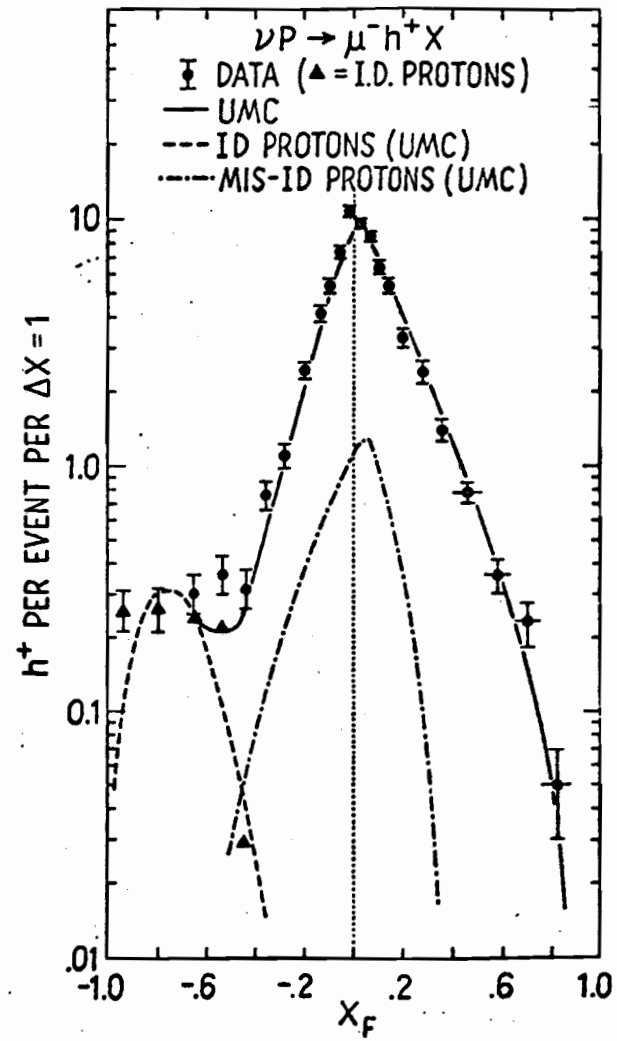
$\nu P \to \mu^- h^+ X$
DATA (▲ = I.D. PROTONS)
UMC
ID PROTONS (UMC)
MIS-ID PROTONS (UMC)
h^+ PER EVENT PER $\Delta X = 1$
X_F

Fig. 9

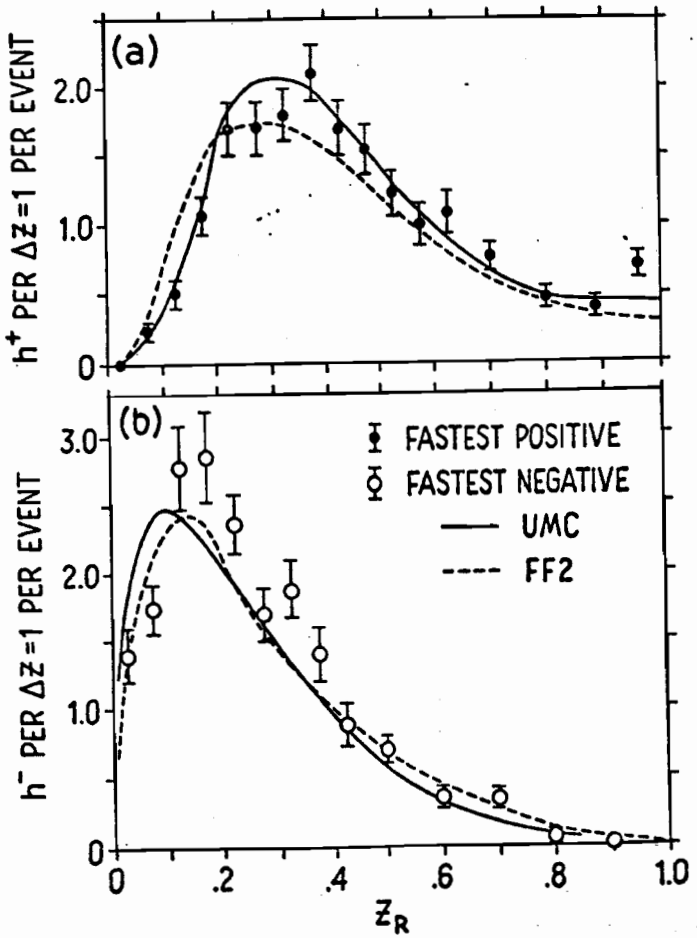
(a)
(b)
h^+ PER Δz=1 PER EVENT
h^- PER Δz=1 PER EVENT
FASTEST POSITIVE
FASTEST NEGATIVE
UMC
FF2
z_R

Fig. 10

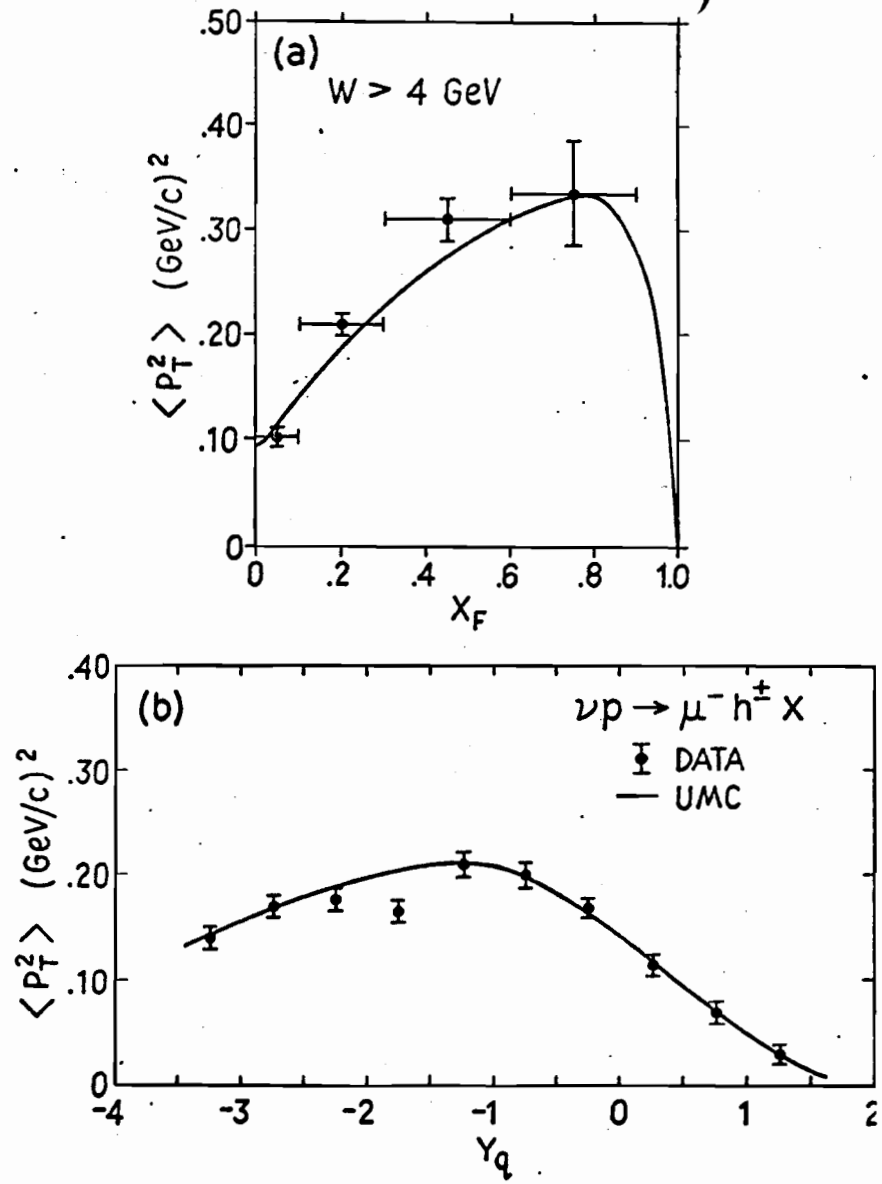
(a)
W > 4 GeV
$\langle p_T^2 \rangle$ (GeV/c)^2
X_F
(b)
$\nu p \rightarrow \mu^- h^\pm X$
DATA
UMC
$\langle p_T^2 \rangle$ (GeV/c)^2
Y_q

Fig. 11

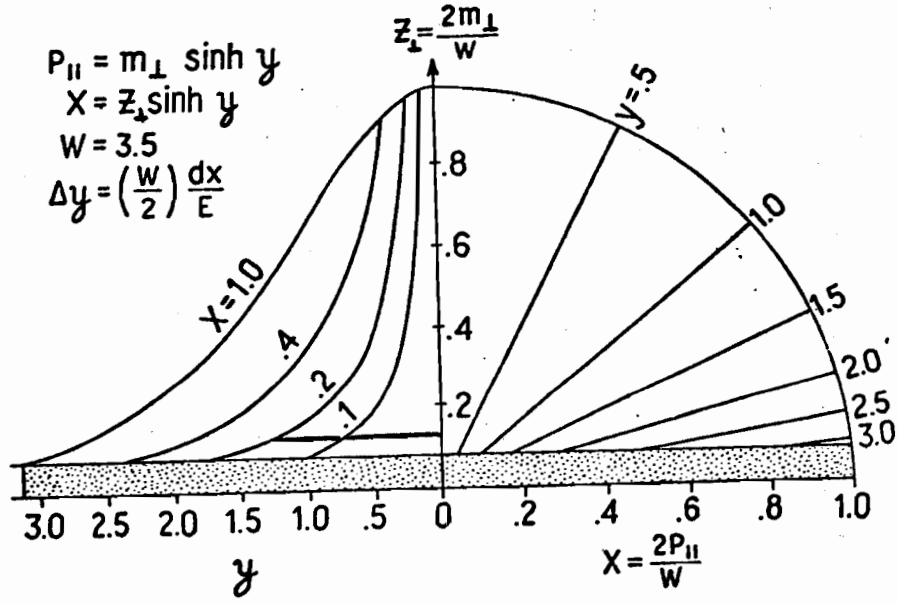
$P_{\parallel} = m_{\perp} \sinh y$
$X = Z_{\perp} \sinh y$
$W = 3.5$
$\Delta y = \left(\frac{W}{2}\right) \frac{dx}{E}$
$Z_{\perp} = \frac{2m_{\perp}}{W}$
$X = 1.0$
.4
.2
.1
$y = .5$
1.0
1.5
2.0
2.5
3.0
.8
.6
.4
.2
3.0 2.5 2.0 1.5 1.0 .5 0 .2 .4 .6 .8 1.0
y
$X = \frac{2P_{\parallel}}{W}$

Fig. 12

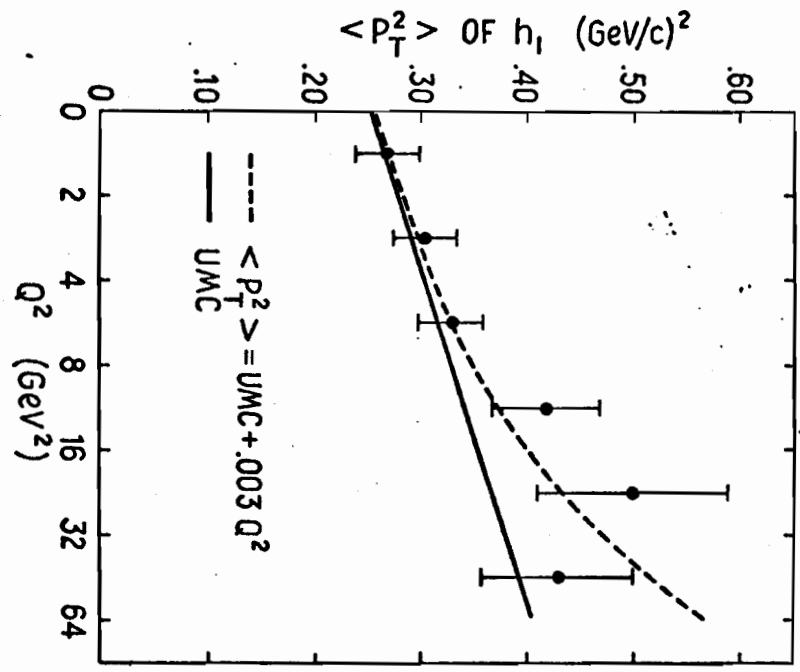
$\langle P_T^2 \rangle$ OF h_1 (GeV/c)^2
0 .10 .20 .30 .40 .50 .60
0 2 4 8 16 32 64
Q^2 (GeV^2)
$\langle P_T^2 \rangle = UMC + .003\, Q^2$
UMC

Fig. 13

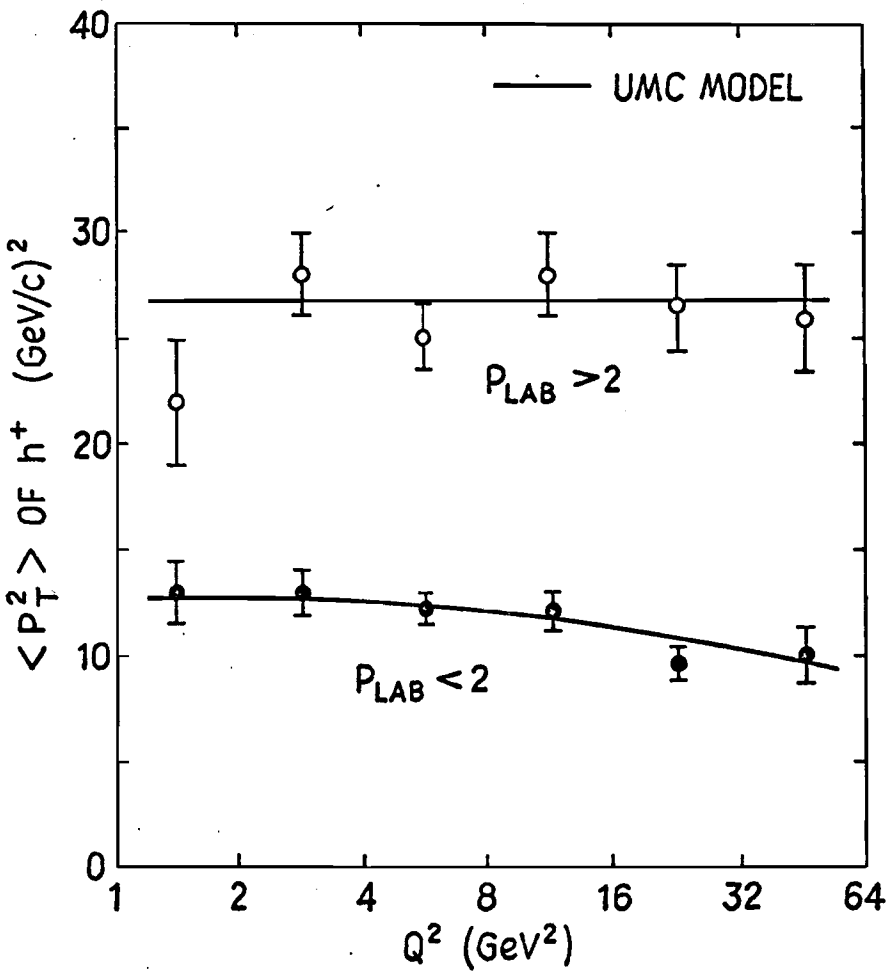
UMC MODEL
$P_{LAB} > 2$
$P_{LAB} < 2$
$\langle P_T^2 \rangle$ OF h^+ (GeV/c)^2
Q^2 (GeV^2)
0
10
20
30
40
1
2
4
8
16
32
64

Fig. 14

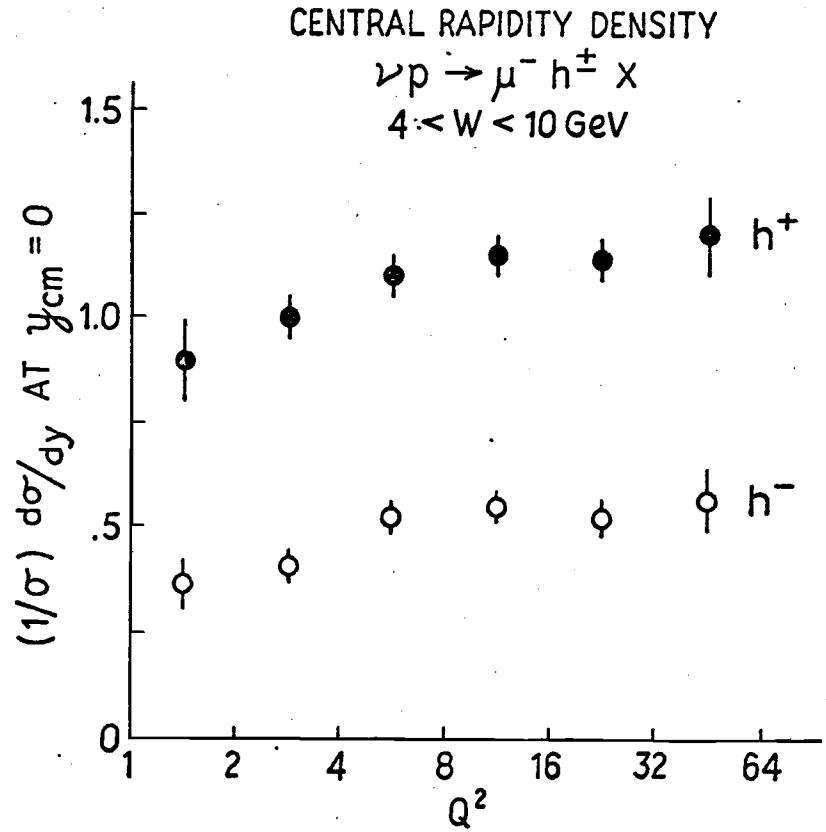
CENTRAL RAPIDITY DENSITY
$\nu p \to \mu^- h^\pm X$
$4 < W < 10$ GeV
$(1/\sigma)\, d\sigma/dy$ AT $y_{cm} = 0$
h^+
h^-
Q^2
0
.5
1.0
1.5
1
2
4
8
16
32
64

Fig. 15